AGU PUBLICATIONS

JGR

Journal of Geophysical Research: Oceans

RESEARCH ARTICLE

10.1002/2014JC010113

Companion to *Matano et al.* [2014], doi:10.1002/2014JC010116.

Special Section:
Early scientific results from the salinity measuring satellites Aquarius/SAC-D and SMOS

Key Points:
- Satellite salinity sensors capture low-salinity detrainment events from shelves
- SW Atlantic low-salinity detrainments cause highest basin-scale variability
- In summer low-salinity detrainments cause extended low-salinity anomalies

Supporting Information:
- Supporting Information
- Figure S1
- Figure S2
- Figure S3
- Figure S4
- Figure S5
- Figure S6

Correspondence to:
A. R. Piola,
apiola@hidro.gov.ar;
R. A. Guerrero,
raul.guerrero@inidep.edu.ar

Citation:
Guerrero, R. A., A. R. Piola, H. Fenco, R. P. Matano, V. Combes, Y. Chao, C. James, E. D. Palma, M. Saraceno, and P. Ted Strub (2014), The salinity signature of the cross-shelf exchanges in the Southwestern Atlantic Ocean: Satellite observations, *J. Geophys. Res. Oceans*, *119*, 7794–7810, doi:10.1002/2014JC010113.

Received 1 MAY 2014
Accepted 13 OCT 2014
Accepted article online 17 OCT 2014
Published online 20 NOV 2014

The salinity signature of the cross-shelf exchanges in the Southwestern Atlantic Ocean: Satellite observations

Raul A. Guerrero[1], Alberto R. Piola[2,3], Harold Fenco[1], Ricardo P. Matano[4], Vincent Combes[4], Yi Chao[5,6], Corinne James[4], Elbio D. Palma[7], Martin Saraceno[8], and P. Ted Strub[4]

[1]Instituto Nacional de Investigación y Desarrollo Pesquero (INIDEP), Mar del Plata, Argentina, [2]Departamento Oceanografía, Servicio de Hidrografía Naval, Buenos Aires, Argentina, [3]Departamento de Ciencias de la Atmósfera y los Océanos, Universidad de Buenos Aires, and UMI/IFAECI, CONICET, Buenos Aires, Argentina, [4]College of Earth, Ocean and Atmospheric Sciences, Oregon State University, Corvallis, Oregon, USA, [5]Remote Sensing Solutions, Inc., Pasadena, California, USA, [6]University of California, Los Angeles, California, USA, [7]Departamento de Física, Universidad Nacional del Sur and Instituto Argentino de Oceanografía, Bahía Blanca, Argentina, [8]Centro de Investigaciones del Mar y la Atmósfera and Departamento de Ciencias de la Atmósfera y los Océanos, Universidad de Buenos Aires, and UMI/IFAECI, CONICET, Buenos Aires, Argentina

Abstract Satellite-derived sea surface salinity (SSS) data from Aquarius and SMOS are used to study the shelf-open ocean exchanges in the western South Atlantic near 35°S. Away from the tropics, these exchanges cause the largest SSS variability throughout the South Atlantic. The data reveal a well-defined seasonal pattern of SSS during the analyzed period and of the location of the export of low-salinity shelf waters. In spring and summer, low-salinity waters over the shelf expand offshore and are transferred to the open ocean primarily southeast of the river mouth (from 36°S to 37°30′S). In contrast, in fall and winter, low-salinity waters extend along a coastal plume and the export path to the open ocean distributes along the offshore edge of the plume. The strong seasonal SSS pattern is modulated by the seasonality of the along-shelf component of the wind stress over the shelf. However, the combined analysis of SSS, satellite-derived sea surface elevation and surface velocity data suggest that the precise location of the export of shelf waters depends on offshore circulation patterns, such as the location of the Brazil Malvinas Confluence and mesoscale eddies and meanders of the Brazil Current. The satellite data indicate that in summer, mixtures of low-salinity shelf waters are swiftly driven toward the ocean interior along the axis of the Brazil/Malvinas Confluence. In winter, episodic wind reversals force the low-salinity coastal plume offshore where they mix with tropical waters within the Brazil Current and create a warmer variety of low-salinity waters in the open ocean.

1. Introduction and Background

Continental runoff discharges freshwater, sediments, organic material, and dissolved substances onto the continental shelf producing a significant impact on the ocean's physical, chemical, and biological properties. Though the input of low-salinity waters into the ocean may cause large-salinity anomalies, the scarcity of in situ data with the required time and space coverage precludes determining their distribution and time variability and the extent of their impact on the physical and biogeochemical properties of the open ocean.

The recent advent of satellite-derived sea surface salinity (SSS) observations provides a unique opportunity to monitor the low-salinity signals in the open ocean and improve the understanding of shelf-deep ocean exchanges. In spite of the relatively low resolution of these data (~100 km) and their relatively short record lengths (2–3 years), a preliminary analysis of the SSS distribution shows that the export of shelf waters to the deep ocean near 35°S creates the largest signal of SSS variability of the subtropical South Atlantic (Figure 1).

The Río de la Plata (hereafter RdlP) drains nearly 20% of the surface area of South America and discharges about 23,000 $m^3\ s^{-1}$ of freshwater on the western South Atlantic shelf at 35°S [*Borús et al.*, 2013]. An additional source of freshwater is the Lagoa dos Patos (LdP), which discharges about 2400 m^3/s [*Vaz et al.*, 2006] at 32°S. An analysis of historical hydrographic data shows that the spatial distribution of buoyant low-salinity waters displays large seasonal fluctuations on the shelf: in late spring and summer the river plume retreats southward to about 32°S and expands offshore reaching the shelf break (Figure 2a) while in austral

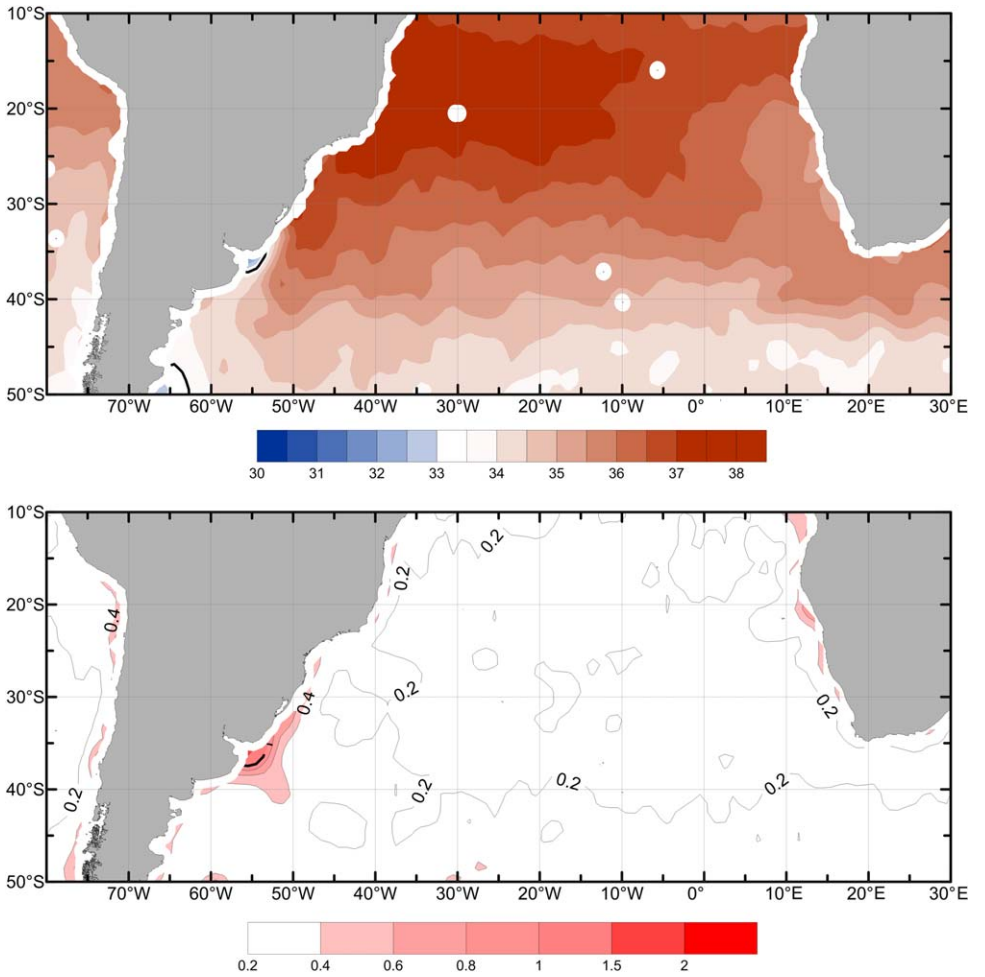

Figure 1. (a) Mean SSS distribution in the subtropical South Atlantic derived from Aquarius L3 monthly gridded (1° × 1°) data product September 2011 to August 2013. (b) Standard deviation of SSS.

fall-winter the RdlP waters spread northeastward along the coast of Uruguay and southern Brazil beyond 28°S (Figure 2b) [*Piola et al*., 2000]. These seasonal oscillations have a profound impact on the shelf ecosystem as far as 1000 km from the river mouth [e.g., *Emilson*, 1961; *Ciotti et al*., 1995; *Stevenson et al*., 1998].

The RdlP outflow mixes with subantarctic shelf water (SASW, SSS ∼ 33.7), which occupies a large fraction of the shelf south of 35°S, and with subtropical shelf water (STSW, SSS ∼ 35), which is found farther north [*Piola et al*., 2000; *Möller et al*., 2008]. Around 37°S a fraction of SASW mixes with the RdlP discharge, leading to a sharp decrease in surface salinity (Figures 2a and 2b). STSW is a mixture of tropical water from the upper portion of the Brazil Current, and several continental discharges, e.g., the RdlP, LdP, the Itajai River, etc. [*Campos et al*., 2013]. STSW occupies parts of the subsurface layer on the narrow shelf off southern Brazil. Plata plume water (PPW), characterized by SSS $<$ 33.5, is formed by mixtures of SASW and STSW to SSS $<$ 33.5 by RdlP discharge [see *Piola et al*., 2000; *Möller et al*., 2008] (S $<$ 33.5 in Figures 2c and 2d).

SASW and STSW form a sharp, nearly density-compensating temperature and salinity transition, referred to as the Subtropical Shelf Front (STSF) [*Piola et al*., 2000]. Historical data indicate that the STSF extends southward from the inner shelf off Rio Grande (∼32°S) and reaching the shelf break near 36°S. The location of the front is apparent in Figures 2e and 2f. The dynamical connection between the STSF and the RdlP plume is poorly understood but observations suggest that the STSF does not undergo the sharp seasonal fluctuations that characterize the SSS distribution over the shelf [*Piola et al*., 2008b].

The circulation over the shelf is largely controlled by the alongshore winds, and the onshore influence of the boundary currents flowing along the continental slope [see *Palma et al*., 2008; *Matano et al*., 2010].

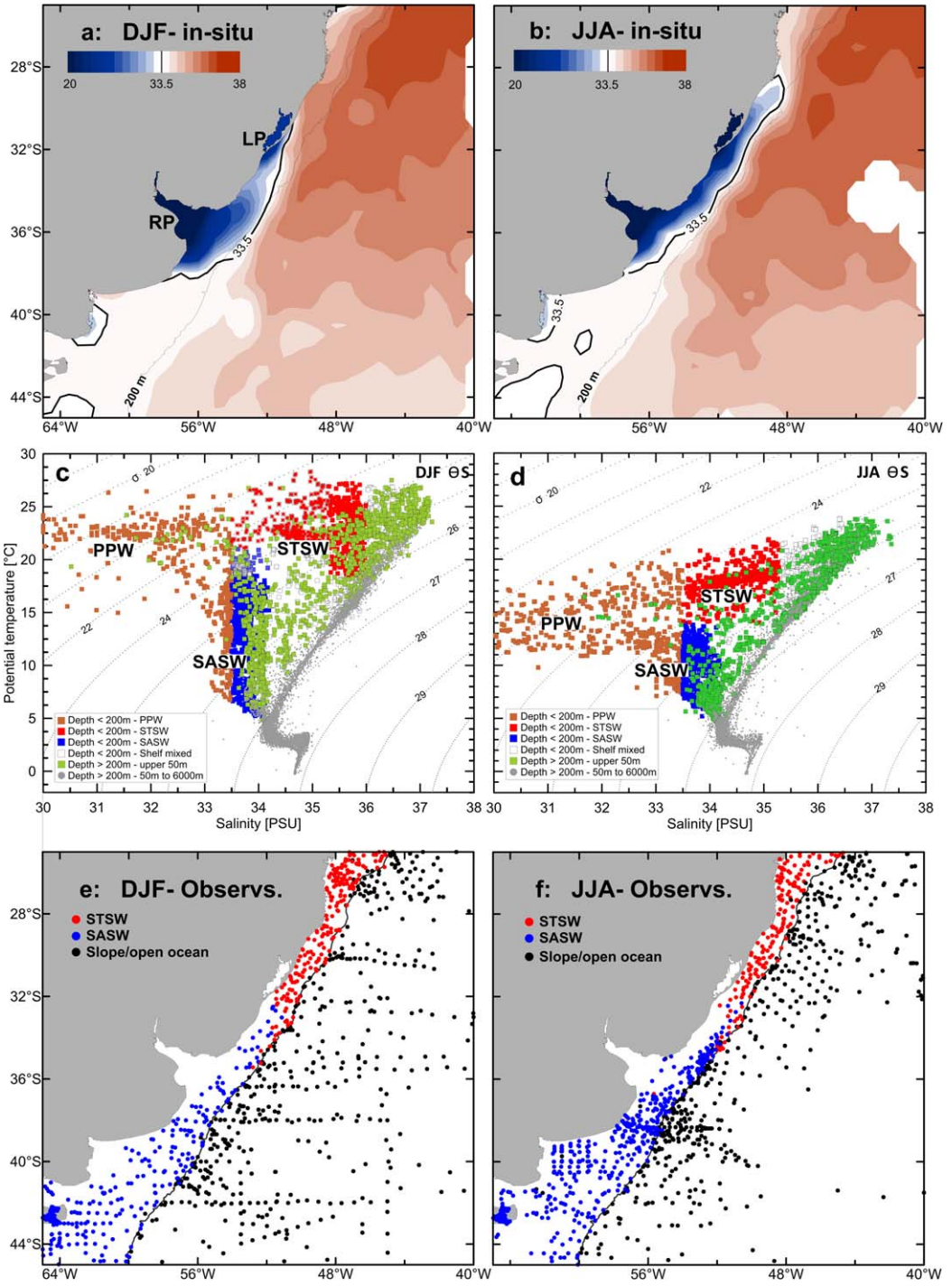

Figure 2. Summer (DJF) and winter (JJA) distribution of SSS from in situ observations (a, b), T-S distributions (c, d), and station distributions (e, f). Shelf water masses described in the text are color coded as follows: subantarctic shelf water (blue), subtropical shelf water (red), and plata plume water (light brown). Green symbols indicate data in the upper 50 m in the open ocean (bottom depth >200 m) and gray symbols data deeper than 50 m. The 200 m isobath (gray thick line) is shown in Figures 2e and 2f, where stations are color coded according to their surface properties.

Seasonal wind reversals over the shelf are associated with the meridional displacement of the South Atlantic midlatitude high-pressure system. Its southward displacement observed in austral summer generates northeasterly winds over the shelf from ~20°S to ~ 40°S. In winter, south of ~31°S the winds reverse to southwesterly, while farther north winds blow from the offshore region [see *Castro and Miranda*, 1998; *Piola et al.*,

2008a]. These southwesterly wind reversals reinforce the intrusion of cold subantarctic waters and the northward extension of PPW in late fall-winter, while the return to northeasterly winds produce a southward retraction and offshore expansion of PPW during spring-summer [*Palma et al*., 2008; *Combes and Matano*, 2014] (Figures 2a and 2b). However, a subsurface penetration of subantarctic waters occurs throughout the year, thus sustaining the STSF [*Palma et al*., 2008]. Based on the sharp transition between SASW and STSW, it has been hypothesized that shelf waters are expelled offshore following the path of the STSF [*Piola et al*., 2008b]. This is in agreement with the observations of low-salinity waters in the Brazil/Malvinas Confluence (BMC) observed on the TS distributions off the 200 m isobaths (green symbols in Figures 2c and 2d), which have been ascribed to export of shelf and RdlP waters [*Gordon*, 1989; *Provost et al*., 1996]. However, the lack of observations has precluded identifying the sources and paths of these waters and the processes that control them.

This paper has two objectives: first we will address the feasibility of using satellite-derived SSS from NASA's Aquarius and ESA's Soil Moisture and Ocean Salinity (SMOS) data to characterize the seasonal and intraseasonal variability of the low-salinity signal in the western South Atlantic shelf and slope during the satellite observation period (2010–2013). To reach this objective we first developed a new processing technique of Aquarius data that improves its time and space resolution and limits land contamination compared with the standard L3 product. This first objective also allows the comparison between SSS-Aquarius and SSS-SMOS. Our second objective is to discuss some of the dynamical processes that may be important in controlling the export of low-salinity shelf waters to the deep-ocean focusing on the analysis of existing satellite and in situ observations. In a companion paper, this analysis is further extended using the results of a numerical model [*Matano et al*., 2014]. This introduction is followed by a description of the data and the processing methods. The results and discussion are presented in sections 3 and 4, respectively, and concluding remarks are presented in section 5.

2. Data and Methods

This study employs historical hydrographic data and river discharge estimates together with satellite-derived sea surface salinity, surface winds, temperature, chlorophyll-a, and currents.

2.1. In Situ Observations

The historical hydrographic data were obtained from holdings at Centro Argentino de Datos Oceanográficos (www.ceado.gov.ar) and Instituto Nacional de Investigación y Desarrollo Pesquero (www.inidep.edu.ar). The data set consists of more nearly 28,000 bottle and CTD profiles mostly collected between 1960 and 2005. Daily RdlP discharge data for the period 2009–2013 were provided by Instituto Nacional del Agua, Argentina [*Borús et al*., 2013].

2.2. Satellite Salinity Data and Processing

This study employs Aquarius and SMOS sea surface salinity data (hereafter referred to as SSS-Aq and SSS-SMOS, respectively). SMOS data encompasses the period from January 2010 to December 2013 and Aquarius data from September 2011 to December 2013. The Aquarius L3 data are limited to SSS >30 and have a resolution of 1 month and $1^\circ \times 1^\circ$. Land contamination limits the radiometer data retrieval nearshore [*Meissner*, 2014], because the target salinity precision of 0.2 requires the integration from the three radiometer beams and poses a serious limitation on the analysis of the effect of continental discharges. To overcome these limitations in the L3 data we have generated a new L3 data product with finer spatial resolution, shorter temporal averaging and a careful selection of data quality flags. This procedure allows us to better resolve the mesoscale variability and to capture low-salinity detrainments from the shelf region. We use Aquarius Level 2 version 2.0 (L2 v2.0) data to construct weekly SSS fields with salinities >20 with a $0.5^\circ \times 0.5^\circ$ resolution. These data were obtained from NASA Jet Propulsion Laboratory (ftp://podaac.jpl.nasa.gov/). Figure 3 presents the austral summer (DJF) and winter (JJA) averaged for 2011–2013. Following *Lilly and Lagerloef* [2008] we applied a Local Polynomial gridding technique with an order 1 polynomial, a Gaussian kernel with a smoothing factor of 0.01, and a variable bandwidth. The bandwidth is determined by the number of observations, $\sim$70 km for 1 week of L2 data. The gridded data are on a $1^\circ \times 1^\circ$ longitude/latitude grid over a weekly time window. Centered on each week a 3 week weighted moving average was applied

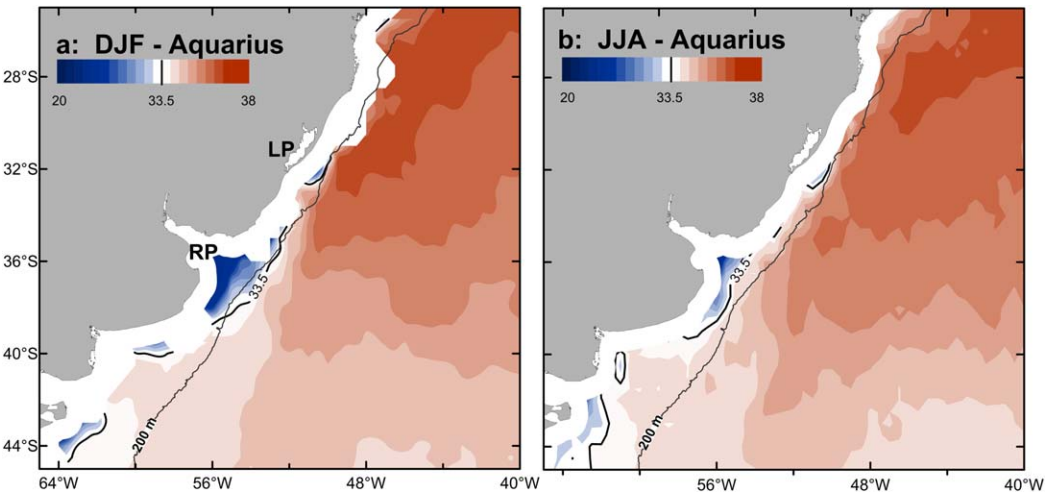

Figure 3. (a) Summer (DJF) and (b) winter (JJA) distribution of SSS from Aquarius reprocessed from along-track L2 data. The gray thick line indicates the 200 m isobath.

with a weight of 0.25 for the side weeks and 0.5 for the center week. Thus, the weekly product is the results of a 3 week average that uses a number of observations similar to the standard Aquarius monthly L3 product in order to maintain an equivalent accuracy, but with a weighting distribution that better represents the SSS patterns observed in the center week. The choice to use Aquarius v2.0, instead of the more recent v2.5.1, is based on the fact that the former better represents the observed salinity over the relatively homogenous Patagonia continental shelf (SSS $\sim$ 33.6–33.8). In addition, version 2.5.1 adjustment of ascending-descending SSS data at track crossovers applied by the Aquarius Validation Data System (AVDS) led to a bias at low salinities (T. Liu, personal communication, 2014). This is in agreement with our own results based on the comparison of 1241 salinity observations from Argo floats available in the South Atlantic with concomitant SSS-Aq at 0.5° $\times$ 0.5° resolution, which for v2.5.1 presents a positive salinity bias of $\sim$0.5 at SSS $<$ 35 (see supporting information Figure S1). While this article was under revision NASA released the Aquarius L3 data version 3.0. We compared the SSS distribution derived from L3 v3.0 data with the v2.0 distribution for the 11 December 2011 (Figure S1). We note that at salinities lower than 35.5 SSS-Aq v2.0 is fresher than v3.0. Moreover, SSS-Aq v2.0 data also compare better with observations over the continental shelf than v3.0, while both data versions are in good agreement at salinities higher than 35 (Figure S1). Despite of these differences, the SSS patterns that emerge from the most recent data set are in good qualitative agreement with the ones derived from v2.0 used in our analysis. Further details on the Aquarius data processing are presented as supporting information.

To describe the high-frequency variability of SSS, we also use along-track Aquarius L2 data from individual beams excluding data within a footprint distance from the coast (Figure 4). Using data from single beams avoids the introduction of errors due to bias between beams. These data allow the construction of low noise time series with weekly resolution. The central positions of all ascending beams: beam 2_1, beam 3, and beam 2_2, hereafter referred to as southern (ST), central (CT), and northern (NT) tracks used in the analysis are shown in Figure 4. Beams 2_1 and 3 correspond to the same Aquarius track, while beam 2_2 is covered on the following path, 3 days later.

SSS-SMOS data are used to cross-validate low-salinity detrainment events from the shelf on the new SSS-Aq weekly fields and to extend the SSS data back to January 2010. To produce SSS-SMOS fields (e.g., Figure 5b) a kriging interpolation method was applied using SMOS L2 9 day weighted average with a time resolution of 3 days, spatial resolution of 0.25° $\times$ 0.25° (http://www.smos-bec.icm.csic.es/), and a search radius of 0.75° $\times$ 0.75°. This interpolation method was used to produce a grid of the same accuracy and spatial resolution and to fill data gaps on the original L2 product, since this technique is optimal, unbiased and minimizes the variance of the estimates.

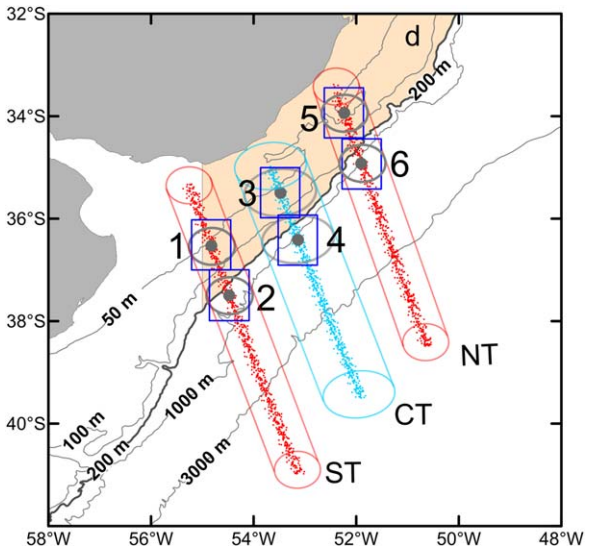

Figure 4. Ground track of Aquarius beam 2: southern and northern tracks (ST and NT) and beam 3 central track (CT) used to characterize the cross-shelf structure of low-salinity detrainments from the continental shelf. Points along each track mark the central position of each data from beam 2 (red) and 3 (light blue). The gray ellipses indicate schematically the extent of the observation for each beam. Points 1, 3, and 5 (2, 4, and 6) indicate the position of the outer shelf (upper slope) time series shown in Figures 7, S5, and S6. The shaded area indicates the region over which the mean wind stress was calculated and shown in Figures 7, S5, and S6. The gray lines indicate the 50, 100, 200 (thick), 1000, and 3000 m isobaths.

2.3. Ancillary Satellite Data

Given the relatively low spatial resolution of satellite-derived SSS, to further evaluate the horizontal patterns of mesoscale features, we analyze ~1/3°, 5 day resolution surface currents from NOAA's Ocean Surface Current Analysis (OSCAR, http://www.oscar.noaa.gov/) for the period 25 November 2011 to 3 January 2012, and 27 May 2010, 25 January 2011, and 12 February 2012. OSCAR is designed to provide operational ocean surface velocity fields from satellite altimeter, vector wind, and sea surface temperature data. The absolute velocity is computed using the mean dynamic height inferred from the World Ocean Atlas [*Bonjean and Lagerloef*, 2002]. In addition, we use a 8–15 December composite SST from NOAA CoastWatch (http://coastwatch.pfeg.noaa.gov/erddap/griddap/) and 3–10 and 11–18 December composites L3 gridded surface chlorophyll-*a* concentration from the Moderate Resolution Imaging Spectroradiometer (MODIS) Aqua (http://oceancolor.gsfc.nasa.gov/cgi/l3). SST and chlorophyll-*a* fields were centered on 11 December 2011 in correspondence with the low-salinity detrainment observed in the satellite-derived SSS. Both SST and surface chlorophyll-*a* are 9 km resolution. In addition, we use weekly maps, 1/3° resolution of absolute dynamic topography (MADT) from the Archiving, Validation and Interpretation of Satellite Oceanographic data (AVISO, http://www.aviso.oceanobs.com) for the period January 1993 to December 2012. MADT are gridded sea surface heights above an estimate of the marine geoid. The dynamic topography is the sum of sea level anomaly (SLA) and mean dynamic topography (MDT), both being referenced over a 20 year period (version v15.0). The delayed-time reference time series of the gridded SLA data have been used. This version merges two satellite missions that cover the same orbits for the entire period. It is, therefore, the most suitable product to build seasonal climatologies. MDT is derived from the combination of Gravity Recovery and Climate Experiment (GRACE) data, altimetry, and in situ observations [*Rio et al.*, 2011]. To analyze the dynamical causes of the observed property distributions we use daily wind observation from the European Advance SCATterometer (ASCAT) for the period January 2008 to December 2013, obtained from the NOAA/NESDIS web site (http://nesdis.noaa.gov). ASCAT gridded wind data were averaged over a region limited by the coast line and the 200 m isobath between 32°S and 55°W (shaded area in Figure 4).

3. Results

3.1. Sea Surface Patterns

To illustrate the spatial patterns of the surface fields obtained with the above described procedures Figure 5a presents the SSS-Aq distribution centered on 11 December 2011. The offshore region is characterized by strong mesoscale eddies. Large warm-salty and cold-fresh core eddies are associated with anticyclonic and cyclonic circulation features, respectively (e.g., A1 and C1-C2 in Figure 5). The SSS-Aq distribution also clearly depicts a detrainment of low-salinity waters from the shelf near 38°S. The SSS-SMOS field (Figure 5b) allows a comparison of both satellite salinity products. The main feature of interest in this study, common in the SSS-Aq and SSS-SMOS fields, is the low-salinity plume extending from the shelf to the open ocean. In both satellite salinity fields this low-salinity filament is connected to the low-salinity region observed over the continental shelf near the mouth of RdlP. The SSS-SMOS distribution presents a more intense salinity

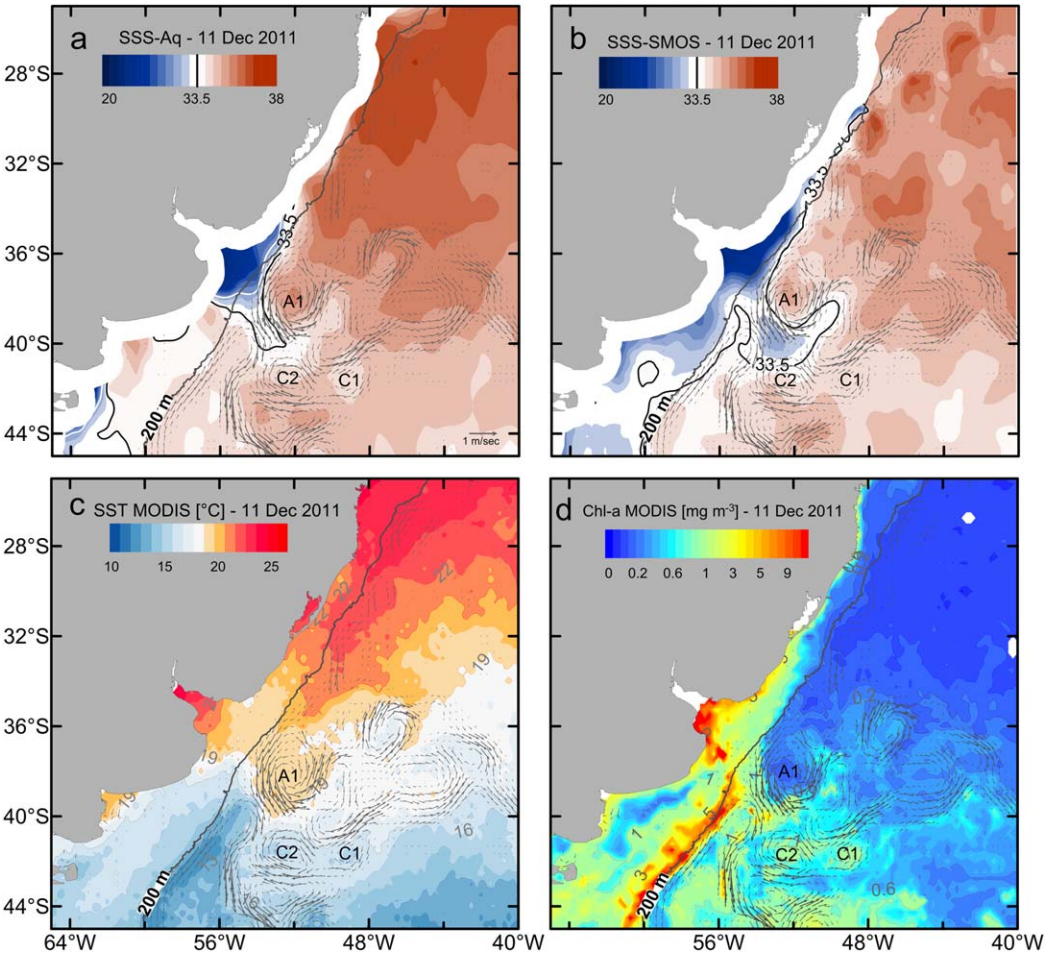

Figure 5. SSS distributions from (a) Aq and (b) SMOS, (c) SST and (d) surface chlorophyll concentration from MODIS Aqua for 11 December 2011. Also shown in each figure are the OSCAR velocities for the same date. The gray thick line indicates the 200 m isobath.

gradient around the edges of this plume, probably due to the shorter time span (9 days for SMOS and 21 days for Aquarius) and to the higher horizontal resolution of the SMOS footprint. In the open ocean the SSS distributions show different patterns, with SSS-Aq presenting a large-scale region of high salinity (~36.5) and SMOS displaying a set of eddy-like high-salinity features surrounded by fresher water (Figures 5a and 5b, supporting information Figures S2c and S2d). In agreement with other studies, in the open ocean SSS-Aq is higher than SSS-SMOS by ~0.5 (Y. Chao, personal communication, 2013). However, at low salinities (SSS $<$ 32) SSS-Aq is lower than SSS-SMOS. Similar SSS-Aq and SSS-SMOS biases have been observed elsewhere (N. Reul, personal communication, 2014). To further compare Aquarius and SMOS salinity data we analyze the differences between SSS-Aq and SSS-SMOS at the selected mid-shelf and slope points (1 through 6 for the period September 2011 to December 2013 (supporting information Figure S3c). Though these differences suggest that SSS-Aq would generally produce higher SSS anomalies associated with the export of low-salinity waters to the open ocean, we note that within the low-salinity detrainments SSS-SMOS is lower than SSS-Aq (i.e., Figures 5a, 5b, S2c, and S2d). We speculate that this may be due to the higher time and space resolution of SSS-SMOS, which appears to better capture the small scale features of the low-salinity detrainments even in the L3 data (see supporting information Figure S3).

The OSCAR surface velocity field of 11 December 2011 is based on observations collected 9–13 December and is overlaid on the above described SSS fields in Figure 5. Figure 5c displays the 8 day composite of SST centered on 11 December 2011. Warm-salty rings and meanders (e.g., SSS-Aq $>$ 35.5 and SST $>$ 19°C, A1) are associated with anticyclonic circulation, while cold-fresh rings and meanders (e.g., SSS $<$ 34.5 and SST $<$ 16°C, C1 and C2) are associated with cyclonic circulation patterns. Figure 5d displays the MODIS Aqua surface chlorophyll distribution constructed from data collected between 3 and 18 December 2011.

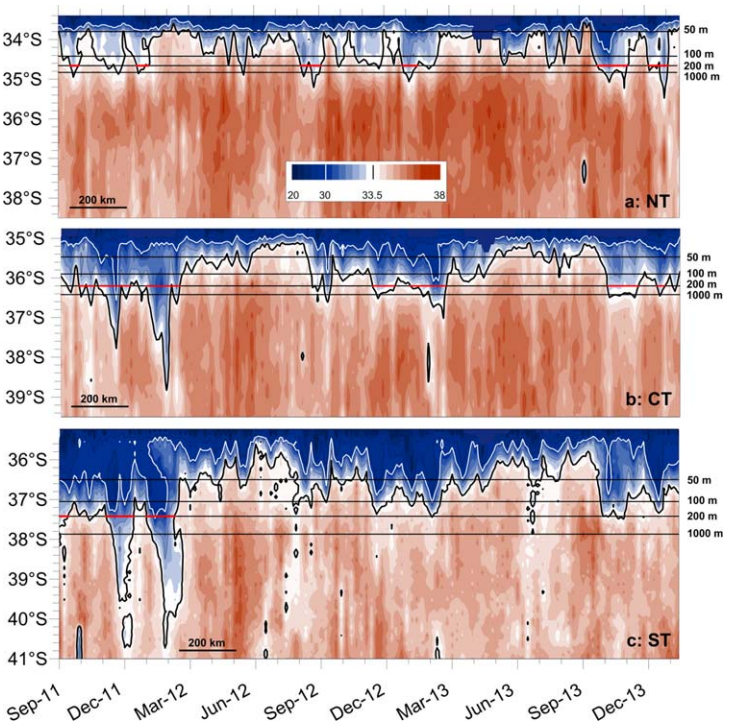

Figure 6. Hovmoller diagrams of SSS-Aquarius constructed from single beam along-track data across the shelf and slope region on (top) northern, (middle) central, and (bottom) southern tracks, see Figure 4 for locations. The heavy black contour is the 33.5 isohaline and the thin white contour the 30 isohaline. Horizontal black lines mark the position of the 50, 100, 200, and 1000 isobaths along each track. The horizontal red segments indicate the 33.5 isohaline crossing the 200 m isobath.

Anticyclonic eddy A1 presents a low chlorophyll core ($<$0.2 mg m^{-3}) while cyclonic eddies C1 and C2 present relatively high chlorophyll cores ($>$1.2 and $>$1.4 mg m^{-3}, respectively). In addition, the Rio de la Plata water is associated with high surface chlorophyll concentration (Figure 5d), presumably due to higher concentration of sediments and suspended matter [e.g., *Piola et al*., 2008a]. This high chlorophyll concentration band is distinct from the elongated maximum observed along the shelf break farther south, which is characteristic of the Patagonia shelf break front [*Saraceno et al*., 2005; *Romero et al*., 2006]. The overall agreement between the OSCAR surface velocity, SST, and chlorophyll distributions and the mapped salinity fields indicates that despite of the low spatial resolution of the satellite-derived SSS, our mapping procedure is able to capture both, the detrainment of low-salinity shelf waters, which is the main focus of the present study, and the complex mesoscale structures characteristic of the BMC. These results indicate that the new satellite-derived salinity data allow mapping of the surface salinity fields and their time variations with unprecedented realism.

3.2. Cross-Shelf Exchanges

Three transects of along-track Aquarius data from beam two-ascending tracks (ST and NT) and beam three-ascending tracks (CT) were selected to describe the high-frequency variability of SSS-Aq and RdlP influence on the mid and outer shelf and upper slope regions (Figure 4). The time evolution of SSS-Aq along these tracks presents high-frequency cross-shelf variability over the continental shelf, which is associated with displacements of the RdlP surface front (Figure 6). This front is identified by a sharp salinity increase from 28 to 32 in scales smaller than 50 km and can be traced by the 30 isohaline (white contour in Figure 6). Surface salinity gradients decrease considerably farther offshore [*Guerrero et al*., 1997], where the inner shelf is occupied by PPW, characterized by a 30–33.5 salinity range [see *Piola et al*., 2008b; *Möller et al*., 2008].

Though the Aquarius time series are still too short to properly describe seasonal changes, during this 28 month period (September 2011 to December 2013), superimposed with the high-frequency cross-shelf variability at ST and CT, the data suggests a seasonal cycle of continental shelf freshening in late Austral spring (November-December) to late summer (February-March) along the Aquarius tracks (Figures 6b and 6c). To corroborate the seasonal variations in the satellite-derived surface salinity records we analyzed the historical hydrographic observations collected between the 50 and 1000 m isobaths (see supporting information Figure S4). The data present large scatter associated with the large-salinity range characteristic of the region. A large number of observations fall within the 33.6–33.8 salinity range (Figure S4c) that characterizes the subantarctic shelf water [*Piola et al*., 2000]. Despite this large variations, in agreement with the satellite observations the monthly mean SSS-in situ are lowest in summer ($<$33) and highest in winter ($>$33) (Figure S4d).

Table 1. Main Characteristics of Offshore Displacements of the 33.5 Isohaline for Aquarius[a]

Aquarius Track	Start Date	Weeks at 200 m	SSS min	SSS mean	Event Number	Overlapped SMOS
Northern (NT)	22 Nov 2011	4.2	33.1	33.4	2A	6S
	3 Jan 2012	3.4	33.0	33.3	3A	7S
	21 Aug 2012	5.0	32.3	33.0	4A	8S
	8 Jan 2013	3.9	32.1	32.8	6A	10S
	8 Oct 2013	7.0	31.6	32.7	7A	11S
	17 Dec 2013	4.9	31.9	33.1	8A	
Central (CT)	8 Oct 2011	7.3	28.6	32.2	2A	5S
	7 Jan 2012	7.7	30.4	31.8	3A	5S
	17 Nov 2012	5.4	32.5	33.0	5A	9S
	19 Jan 2013	8.1	30.6	32.4	6A	
	19 Oct 2013	7.2	32.6	33.0	7A	11S
	28 Dec 2013	2.6	32.5	33.0	8A	
Southern (ST)	1 Sep 2011	2.9	32.9	32.9	1A	5S
	19 Nov 2011	6.5	31.1	31.9	2A	5S
	14 Jan 2012	6.6	29.8	31.4	3A	5S

[a]Aquarius Track (see Figure 4 for location); Start date: Starting date; Duration: Event duration; Smin: Minimum Salinity recorded over the 200 m isobath; SSmean: Mean Salinity during the Event; Overlapped SMOS: Aquarius Events overlapped with SMOS (SSS less than 33.5 in the SMOS time series).

The cycle in SSS-Aq is significantly weaker in the northern track (Figures 6a and S6a). On the continental shelf, onshore of the 200 m isobath, low-salinity waters (SSS $<$ 33.5) are observed from September 2011 to February 2012, from August 2012 to April 2013, and from October 2013 to the end of the record (January 2014). Conversely, salty water intrusions on the continental shelf occur from March to July 2012 and from April to September 2013. During these periods the low-salinity waters are restricted to shallow areas ($<$50 m on ST and NT and $<$100 m on CT), probably within a continuous coastal band that is presumably connected to the RdlP mouth, as suggested by Figure 2b [*Piola et al*., 2000]. This seasonal oscillation of the surface salinity field at the RdlP mouth is consistent with surface salinity patterns described from in situ observations [*Guerrero et al*., 1997; *Framiñan et al*., 1999] (Figure S4d) and modeling studies [*Simionato et al*., 2001, 2004]. Similar seasonal and interannual oscillations have also been described at a regional scale based on the analysis of historical hydrographic data and numerical simulations [*Piola et al*., 2000, 2005; *Palma et al*., 2004, 2008; *Pimenta et al*., 2005]. All these studies concluded that the seasonal reversal of the alongshore wind is the main forcing leading to the variations in the distribution of low-salinity waters over the shelf.

During the freshening periods along ST and CT, the SSS-Aq data also reveal large-amplitude offshore displacements of low-salinity waters extending beyond the 200 m isobath (Figures 6b and 6c). Some of these features represent outstanding detrainment events of low-salinity water which have not been previously reported. Table 1 summarizes the offshore displacements of the 33.5 isohaline beyond the 200 m isobath (events 1A–8A) identified from the analysis of along-track SSS-Aq data (Figure 6). Similarly, Table 2 summarizes the offshore displacements of low-salinity waters (1S–11S) based on the analysis of SSS-SMOS $<$ 33.5 at slope points 2, 4, and 6 (Figure 4).

Eight offshore displacements of surface waters with SSS $<$ 33.5 across the 200 m isobath were observed during the analyzed Aquarius record (Table 1). On average these events lasted more than 5 weeks with a mean salinity $<$33. The central and northern tracks present six events each, five of which are due to single low-salinity detrainments captured on both tracks (see event number in Table 1). The freshest and most extended events are observed on CT (on average $\sim$6.4 weeks, SSS $\sim$ 32.6, Table 1). Events 2A and 3A, the most intense in the record, observed in December 2011 and February 2012, respectively, are present in all three tracks but show significantly stronger salinity signals at ST and CT (see Table 1). In late November-early December 2011 along ST a plume of low-salinity waters ($<$33.5) extends 500 km into the BMC (Figure 6c). This event also clearly manifests as a 300 km low-salinity intrusion along CT (Figure 6b) where it is associated with low-salinity ($<$30) intrusions observed over the shelf in November 2011 and January 2012. The inner shelf low-salinity features are also apparent along all three tracks, suggesting that the low-salinity waters extend simultaneously over more than 300 km along the shelf and the shelf break. Somewhat less pronounced detrainments are observed in austral spring and summers of 2012–2013 and 2013–2014. Eleven events were identified from the SMOS time series (Table 2), 1S through 4S are observed prior to the date when Aquarius became operational and 5S through 11S are contemporary with Aquarius. The average duration of the SMOS events is longer than the Aquarius events because SMOS is fresher at salinities $\sim$33.5

Table 2. Main Characteristics of Offshore Displacements of the 33.5 Isohaline for SMOS

SMOS Region	Start Date	Weeks S < 33.5	SSS Min	SSS Mean	Event Number	Overlapped Aquarius
Northern (point 6)	9 Feb 2010	3.7	33.0	33.2	1S	
	7 May 2010	8.4	32.5	32.9	2S	
	11 Aug 2010	16.0	32.1	32.9	3S	
	12 Dec 2010	6.3	32.5	32.9	4S	
	17 Sep 2011	6.0	32.5	33.0	5S	1A
	22 Nov 2011	2.1	33.1	33.2	6S	2A
	25 Dec 2011	3.7	33.0	33.3	7S	3A
	12 Ago 2012	4.6	32.7	33.0	8S	4A
	25 Nov 2012	2.6	32.8	33.1	9S	
	22 Dec 2012	5.0	32.8	33.0	10S	6A
	6 Sep 2013	11.4	32.7	33.0	11S	7A
Central (point 4)	19 Jan 2010	7.9	32.7	32.7	1S	
	3 Jun 2010	2.6	33.1	33.1	2S	
	19 Sep 2010	5.6	32.4	32.4	3S	
	6 Dec 2010	15.0	31.7	31.7	4S	
	5 Sep 2011	24.0	31.0	31.0	5S 6S 7S[a]	1A 2A 3A
	13 Nov 2012	15.1	32.3	32.3	9S	5A
	6 Sep 2013	11.9	32.6	32.6	11S	8A
Southern (point 2)	9 Feb 2010	4.1	32.8	33.2	1S	
	10 Oct 2010	2.5	33.2	33.3	3S	
	18 Dec 2010	13.7	31.0	32.2	4S	
	2 Oct 2011	26.3	30.6	32.5	5S 6S 7S[a]	1A 2A 3A
	16 Nov 2012	5.1	32.6	33.0	9S	7A

[a]Events 5S, 6S, and 7S observed at the central and southern regions correspond to a single event lasting at least 24 weeks. SMOS time series at slope Points 2, 4, and 6 (See Figure 4 for Location); Start Date: Starting date; Duration: Event duration; Smin: Minimum Salinity recorded; Smean: Average Salinity during the event; Overlapped Aquarius: SMOS Events overlapped with Aquarius (33.5 Isohaline across the 200 m Isobaths in the Aquarius time series).

(see supporting information Figure S3c and section 4). This is illustrated by event 5S, at points 2 and 4, where SMOS data indicate a continuous detrainment that lasted several months while based on Aquarius data three different events are detected (1A, 2A, and 3A). Three additional SSS distributions based on SMOS and Aquarius data have been mapped and presented in supporting information to further illustrate the sea surface salinity patterns of other detrainment events (2S, 4S, and 7S–3A; Figure S2).

3.3. Dynamical Analysis

To investigate the possible causes of the observed SSS-Aq variability, we analyze the time series of RdlP discharge and alongshore wind stress together with the SSS-Aq at selected locations on each track over the outer continental shelf (gray points 1, 3, and 5 in Figure 4) and over the upper slope (points 2, 4, and 6 in Figure 4). To extend the period of analysis we include SSS-SMOS data over the same regions spanned by each Aquarius point (Figure 4). Each point represents the mean salinity observed by Aquarius within the corresponding elliptical foot print (gray circles in Figure 4), while the SSS-SMOS observations are extracted from an area of 1° latitude × 0.8° longitude at 3 day intervals (blue squares in Figure 4). The data were smoothed with 3 week moving average to minimize the effect of errors in instantaneous SSS observations. The following discussion is based on the analysis of the SSS-Aq time series on CT (points 3 and 4) as this track presents the most intense variability (see Figure 7).

Figures 7a and 7b present the weekly SSS-Aq and 3 day SSS-SMOS time series constructed from the shelf and slope points over CT. Shaded bands in Figures 7, S5, and S6 indicate the timing of the low SSS detrainment events. The time series at ST and NT are presented in supporting information Figures S5 and S6. Figure 7c presents the along-shelf component of the ASCAT wind stress averaged over the shelf NE of the RdlP estuary (Figure 4). The wind stress data was low-passed filtered using a Kaiser filter [*Hamming*, 1977] with a cutoff frequency of 25 days. Also shown in Figure 7c is the along-shelf ASCAT wind stress estimated by averaging the daily records during 2008–2013. The 2008–2013 mean displays a well-defined reversal from southwesterlies to northeasterlies in late September and a return to southwesterlies in mid-March. Figure 7d presents the wind stress anomaly of the observed wind relative to the mean annual cycle, while the daily discharge of RdlP is also presented in Figure 7e.

To determine the possible relationship between wind stress, river outflow, and SSS variability, we calculated the correlation coefficients at points 1–4. Except for point 2 (upper slope, ST) SSS-Aq are significantly correlated with the alongshore wind stress at zero lag and 99% confidence level ($r > 0.64$). At point 2 the correlation with wind

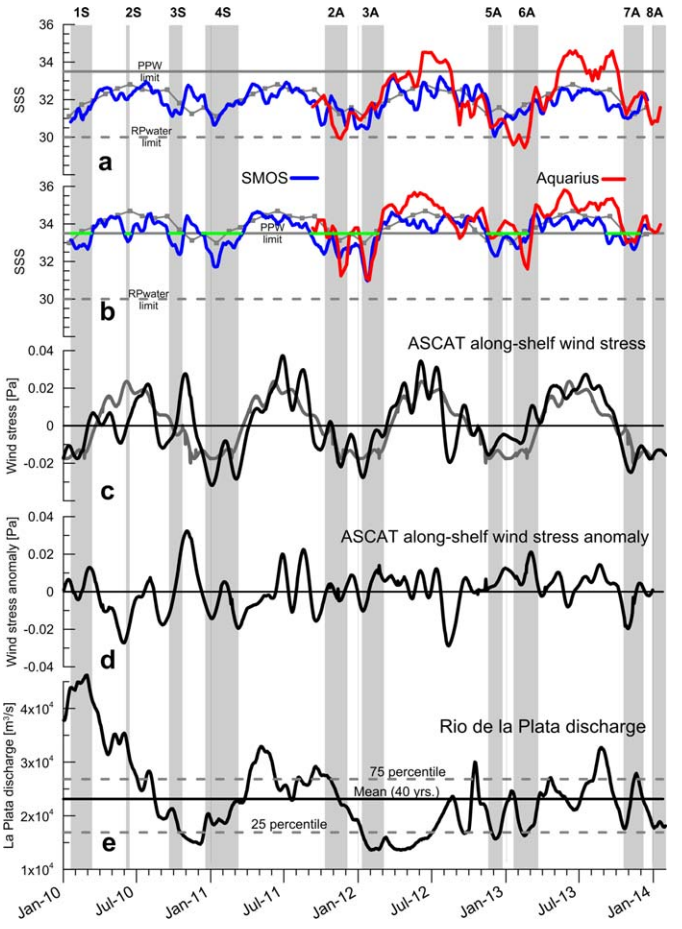

Figure 7. Times series of SMOS (blue) and Aquarius (red) SSS at (a) selected outer shelf (point 3 in Figure 4) and (b) upper slope (point 4 in Figure 4) locations on the central track, beam 3. The horizontal green lines in Figure 7b indicate periods when SSS-SMOS $<$ 33.5 at point 4. The dashed gray lines mark the 30.0 isohaline, which indicates the outer limit of RdlP waters, and the solid gray lines the PPW limit (33.5). (c) ASCAT alongshore wind stress (black) and 2008–2013 mean wind stress (gray) and (d) wind stress anomaly. (e) Plata river discharge. The solid horizontal line indicates the climatological mean (24,045 m^3/s [*Jaime and Menendez*, 2002] for the period 1972–2001) and the dash lines are the upper and lower 75 and 25 percentiles, for the same period, respectively [from *Guerrero et al*., 2010]. SSS data have been smoothed with a moving average of 3 weeks and wind stress data were low-passed filtered with a cutoff frequency of 25 days. The gray background bars mark the periods of detrainment events indicated in Table 1. The time series on Northern and Southern Tracks are shown in supporting information Figures S5 and S6.

stress is somewhat lower (0.51), indicating that the SSS variability is influenced by mesoscale variations of the location of the Brazil/Malvinas Confluence [e.g., *Saraceno et al*., 2004]. At all points the correlation coefficients between SSS and river outflow are lower but increase ($\sim$0.4) when SSS lags the alongshore wind stress by 10–11 weeks. These results are in good qualitative agreement with previous results based on the analysis a SSS proxy determined from 8 years of satellite color data [*Piola et al*., 2008a] and with the second mode of SSS variability in a numerical simulation [*Matano et al*., 2014].

The salinity time series over the shelf (Figure 7a) displays four strong oscillations in the 4 year period between $\sim$29 and 34. Fresh RdlP waters (SSS $<$ 30) dominate in spring and summer while PPW (30 $<$ SSS $<$ 33.5) is present during autumn and winter. The SSS variability over the shelf based on the analysis of a large hydrographic data base has been attributed to a seasonal NNE-SSW (along-shelf) oscillation of the wind stress [*Piola et al*., 2005] and not to an increase in river discharge. In agreement with this result, the wind stress time series (Figure 7c) shows periods with northeasterly (negative) wind stress matching the presence of low-salinity water on the shelf and periods of southwesterly (positive) wind stress during the period when salty waters prevail. In contrast, the RdlP discharge does not present a strong seasonal cycle (Figure 7e). Moreover, though the outflow was lower than average during most of 2012 and early 2013 (Figure 7e), SSS-Aq presents a well-defined minimum in early 2013 (red lines in Figures 7a and 7b).

In autumn and winter positive wind stress forces low-salinity waters northeastward, and forms a coastal low-salinity current [see *Palma et al*., 2008]. Under this condition, the mid-shelf and shelf break are occupied by salty waters (SSSAq $>$ 32–33), which are evident at ST and CT (Figures 6b and 6c). In contrast, negative (northeasterly) wind stress in spring and summer act to transport (Ekman dynamics) the low-salinity water from the RdlP to the area offshore from the estuary (SSS $<$ 31). At this time of the year the low-salinity waters spread offshore reaching the middle and outer shelf also along the southern and central tracks (see Figures 6b and 6c).

The seasonal cycle is conspicuous over the upper slope on the central track (Figure 7b), while the southern track presents significant lower salinity water in the austral spring and summer of 2011–2012 (Figures 6c and S5). Offshore detrainments of low SSS from the shelf to the open ocean are observed during this period (events 2A and 3A in Table 1). The SSS-Aq time series at CT and ST (Figures 7b and S5) suggest that these

events evolved in sequence from the shelf to the slope and from north to south, and reached their maximum detachment on the southern track (Figure 6c). Both events occur ~1 week after a northeasterly wind maximum (Figure 7c). The remaining events reported in Tables 1 and 2 seem to occur after the wind stress reverses to NNE (e.g., August 2012 and October 2013). The spring 2011 and summer 2012 show low-salinity detrainments preceded by a relatively large RdlP discharge, although not significantly exceeding the 75% percentile. The RdlP discharge during the rest of the Aquarius period oscillates around or below the mean, except for two short high discharge periods observed in October 2012 and August 2013 (discharge higher than the 75% percentile, Figure 7d) that preceded events 5A and 7A by 14 and 6 weeks, respectively.

The SMOS time series overlapping the Aquarius period presents the same six events observed on the Aquarius central track (Table 2, CT and Figure 7b) but the SMOS signal is less intense because, as stated earlier, SMOS is saltier than Aquarius at low salinities (Figure S3c), and fresher than Aquarius at higher salinity (see Figures 5a, 5b, S2c, and S2d). Further analysis of the difference between SSS-Aq and SSS-SMOS is presented in supporting information Figure S3. The SSS-SMOS time series reveals four additional detrainment events of low-salinity waters beyond the shelf break and upper slope (Table 2 and Figure 7b). Events 1S and 4S occurred during the spring-summer period in correspondence with the reversal of the alongshore wind stress in spring-summer, while events 2S and 3S occurred during May–June and October 2010. The later events are associated with exceptional winter-early spring reversals of alongshore wind stress. During these periods, particularly in early 2010, the RdlP discharge exceeded 30×10^3 m^3 s^{-1}.

The largest detrainments observed in the upper slope SSS time series (Figure 7b) occurred in December–January–February 2010–2011, December–January–February 2011–2012, and January–February 2013. It is also observed that these large-amplitude events occurred under different discharge conditions; after 4 months of low discharge during the 2010–2011 events, after 4 months of sustained high discharge in 2011–2012, and after 4 months of highly variable discharge in 2013. Thus, these observations further suggest the relatively minor role played by the magnitude of the continental discharge in modulating the detrainment of low-salinity waters from the continental shelf.

3.4. Evolution of an Intense Low-Salinity Detrainment Event

The low-salinity detrainment event observed in December 2011 is clearly displayed on the Aquarius and SMOS SSS distributions (Figures 5a and 5b). This event was preceded by a period of relatively high outflow (Figure 7e) and northeasterly winds (Figure 7c). The detailed evolution of this low-salinity detrainment event is presented in Figure 8. On 27 November, the 33.5 isohaline is located 150 km offshore from the 200 m isobath and extends more than 300 km along the shelf break (Figure 8a). The OSCAR surface current field reveals a strong southward flow (~1 m s^{-1}) over the eastern edge of the low-salinity cell at 37°S. On 4 December the low-salinity waters develops into a plume extending 220 km southeastward from the shelf break near 39°S (Figure 8b), while the surface currents present a strong southeastward flow. At this time the low-salinity waters appear to be advected southward and offshore along the western and southern edges of anticyclonic eddy A1 (Figures 8b and 8c). On 11 December the low-salinity tongue extends further offshore (350 km) and a salty eddy (SSS > 35.5) develops northeast of the plume with the low-salinity water being advected around the eddy rim (Figure 8c). The eddy to low-salinity filament transition is associated with a salinity contrast ~2. The eddy persists in the following weeks while by 1 January the low-salinity signal weakens significantly (SSS > 34.0) as it mixes with the salty background waters (Figures 8d–8f). By 18 December an additional anticyclonic eddy develops centered near 44°S–53°W, whose core is also characterized by high salinity (Figures 8d–8f). The extreme low in SSS-Aq and their off shelf advection from November 2011 to February 2012 (Figures 6b and 6c), are consistent with relatively strong and persistent northeasterly winds over the shelf (Figure 7c) and the development of an intense anticyclonic ring offshore (A1 in Figure 8). Though the SMOS time series do not reproduce the December 2011 event as strongly as Aquarius, a similar low-salinity detrainment also associated with strong northeasterly wind events is observed in the SMOS data in January 2011 (Figures 7b and 7c). This event, however, was preceded by five months of lower than averaged river discharge (Figure 7e).

4. Discussion

4.1. Seasonal Variability

The satellite-derived SSS variability over the outer shelf and slope between 33°S and 37°S (Figures 6 and 7a) shows a well-defined seasonal cycle for the period January 2010 (SMOS) and September 2011 to

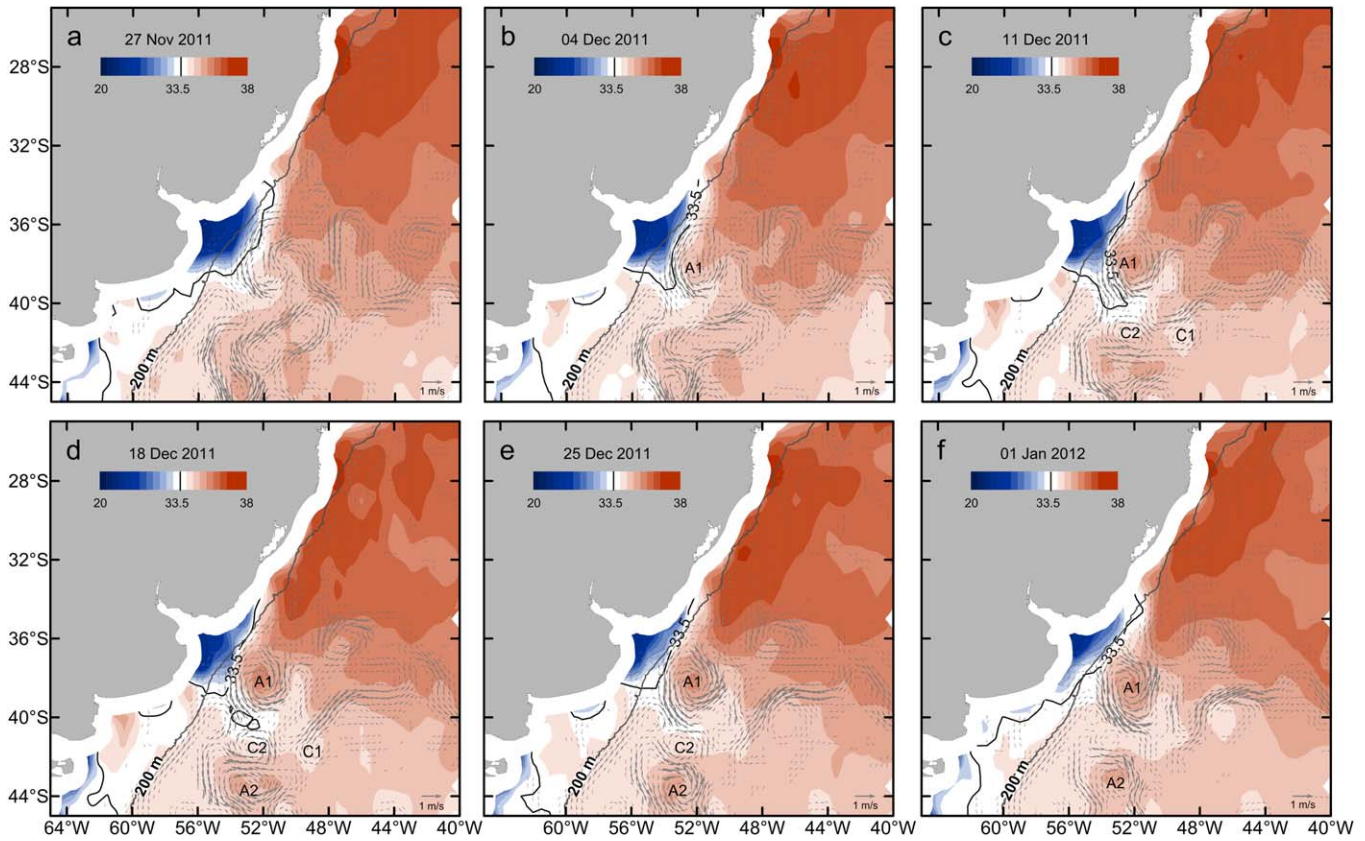

Figure 8. Evolution of SSS-Aq from 27 November 2011 to 1 January 2012 overlapped on OSCAR current vectors, scale shown in lower right-hand side on each panel. The gray thick line indicates the 200 m isobath.

December 2013 (Aquarius). The salinity variations over the outer shelf region are validated by the analysis of historical in situ data (Figures 7, S4, S5, and S6), with low-salinity PPW expanding offshore in austral summer and contracting onshore in winter (Figure 6). These changes in the width of PPW east of the river mouth are consistent with observations and numerical simulations. Two hydrographic surveys carried out in late August 2003 and February 2004 provided the first synoptic distributions of water masses over the continental shelf between 38°S and 27°S [*Campos et al*., 2008]. A volumetric water mass analysis of these data showed that in summer waters with higher than 50% concentration of PPW extend ∼280 km offshore from the estuary mouth and beyond the 200 m isobath near 37°S [*Möller et al*., 2008]. In contrast, in winter the PPW contracts onshore forming a narrow (∼60 km) coastal band that extends northward beyond 28°S [see *Möller et al*., 2008, Figure 12]. During these surveys the extent of PPW closely followed the 32 isohaline and indicate large seasonal SSS changes in the outer continental shelf. Though land contamination prevents observing the PPW distribution in winter based on satellite data (e.g., Figure 3b), the SSS in the outer shelf region presents low-salinity waters (SSS-Aq < 32) prevailing in late spring and summer, when PPW expands offshore (Figure 7a). The analysis of in situ observations [*Piola et al*., 2005], SSS proxies [*Piola et al*., 2008a], and several numerical experiments [*Pimenta et al*., 2005; *Palma et al*., 2008; *Combes and Matano*, 2014; *Matano et al*., 2014] indicate that the seasonal SSS variability is associated with a seasonal reversal of alongshore winds (Figure 7c). The above observations are also in good qualitative agreement with the earlier climatological SSS distributions characteristic of austral winter and summer derived from the analysis of hydrographic data [*Piola et al*., 2000] (see also Figures 2a and 2b).

The pattern of seasonal SSS variability is also apparent further offshore, in the upper slope (Figures 7b, S5b, and S6b), with higher (lower) salinities observed in winter (summer). As a result of mixing between shelf and open ocean waters the amplitude of seasonal SSS variations over the slope are smaller than in the outer shelf (Figures 7a and S5a). However, at this location there are large departures caused by low-salinity events, which are discussed in more detail in a following section. Similar offshore expansions of low-salinity waters

beyond the 200 m isobath in summer and onshore contractions and alongshore extensions in winter are observed in SSS distributions derived from high-resolution numerical models forced by tides, freshwater discharges, offshore boundary currents and June and January climatological winds, respectively [*Palma et al*., 2008]. This evidence indicates that the satellite SSS sensors capture the strong seasonal signals associated with expansions and contractions of the low-salinity waters derived from the Rio de la Plata as they manifest in the outer shelf (Figures 3a and 3b).

Though a detailed comparison between SSS-Aq and SSS-SMOS is beyond the focus of this study we analyze the SSS difference between both sensors during the overlapping period (September 2011 to December 2013) using data at six points (see Auxiliary Material). This analysis shows that SSS-SMOS is lower than SSS-Aquarius at high salinities and higher at low SSS. This results in reduced amplitude of the seasonal cycle in SSS-SMOS data. Consequently, SSS-SMOS presents a negative bias in austral winter (relatively low SSS in the outer shelf) compared to SSS-Aq, while in summer (at low SSS) the data from both sensors are in relatively good agreement (Figure 7a). Regardless of the SSS-Aq and SSS-SMOS discrepancies, the outer shelf data derived from both sensors clearly present seasonal variations in overall agreement with existing observations and models.

4.2. Intraseasonal Variability

Data from both satellite sensors present substantial intraseasonal variability in the outer shelf and upper slope (Figures 7a and 7b). The most conspicuous manifestations of intraseasonal variability of SSS in the upper slope are the low-salinity detrainment events described in section 3 (Figures 6, 7, and S5, and Tables 1 and 2). The Hovmöller diagrams constructed with Aquarius along-track SSS data along CT and ST (Figures 6b and 6c) and the SSS-Aq distributions (Figures 8 and S2) show that these events can drive low-salinity waters (SSS-Aq $<$ 33.5) several hundred km away from the shelf. This is in agreement with earlier observations of low-salinity surface water near the BMC. Based on the analysis of hydrographic data collected in October 1984, *Gordon* [1989] noted that low-salinity waters, which were too warm to be derived from the Malvinas Current, formed elongated filaments or "cells" along the Confluence and suggested that they were first advected offshore by the cyclonic loop described by the Malvinas Current near 39°S, and southward by eddies and filaments of the Malvinas Return Current. Similarly, *Provost et al*. [1996] observed low-salinity waters along the BMC, presumably derived from the Rio de la Plata and extending about 500 km away from the estuary. SSS distributions derived from high-resolution numerical models also suggested the offshore advection of low-salinity plumes at the BMC [*Palma et al*., 2008]. Though none of these data allowed mapping the extent or precisely determining the source of the anomalous waters, the SSS-SMOS and SSS-Aq distributions (Figures 5a, 5b, and 8) clearly indicate that the lowest-salinity waters (SSS $<$ 33.5) are derived from the Rio de la Plata. Moreover, our analyses suggest that these waters are advected away from the shelf region via the BMC and that the export events occur primarily during the austral summer (Tables 1 and 2). The export of shelf waters in summer creates an extensive region of negative salinity anomalies relative to the record length mean (2012–2013), which extends ∼320 km southeastward form the shelf break (Figure 9). The summer anomalies detrain from the shelf near 37°S (Figure 9), in close agreement with the concentrated exit point of particles released in a numerical simulation [*Matano et al*., 2014]. On average, in summer the path of these low-salinity waters closely follows the BMC as revealed by the summer mean dynamic topography (40–50 cm contours in Figure 9).

From data collected in October 1984, *Gordon* [1989] also noted the presence of a warmer variety of low-salinity waters on the western branch of the Brazil Current, which he suggested were originated further north, either by excess precipitation over the coastal region or as a result of northward flow of RdlP waters along the coast which were then diffused offshore, forming a low-salinity cap over the southward flowing Brazil Current. The two varieties of low-salinity waters were also apparent in observations collected in winter 2003. These data presented several warm-fresh (∼15–17°C, $<$34) filaments detaching from the RdlP coastal plume near 29°S and 31°S and a significantly colder variety (∼11°C) close to the Confluence [*Piola et al*., 2008b]. These data suggested that in winter, when under the sustained influence of southwesterly winds the RdlP plume is well-developed as a narrow coastal band extending northeastward from the river mouth, the primary export route of low-salinity waters is along the offshore edge of the plume. The winter 2003 survey further indicates that as these waters mix with the salty Brazil Current they rapidly lose their low-salinity signal [*Piola et al*., 2008b]. Similar detachments of low-salinity waters are suggested by the trajectories of particles released in a numerical model [*Matano et al*., 2014]. On the other hand, the hydrographic data

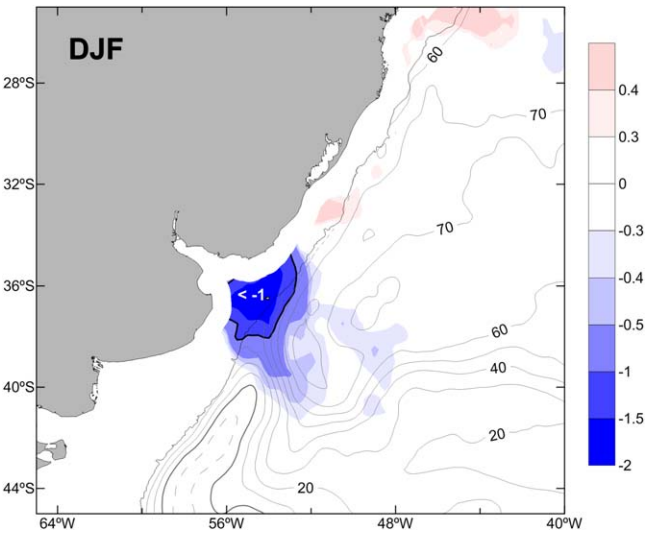

Figure 9. Mean SSS anomaly (colors) and mean dynamic topography (contours, cm) for December–January–February. The salinity anomaly is relative to the 2012–2013 mean. The gray thick line indicates the 200 m isobath.

collected further south across the BMC shows that the cold variety of low-salinity waters is mostly composed of undiluted SASW from the northern Patagonia continental shelf [*Piola et al*., 2008b, their Figure 11]. Though SASW is ∼0.3 fresher than surface waters within the Malvinas Current (SSS $>$ 34), the salinity difference is probably too small for clear detection by the satellite sensors. Thus, in winter, the export of PPW waters and undiluted SASW create a salinity signal much weaker than in summer. These results explain why only three low-salinity export events apparent in the satellite data are observed in winter (2S in April–June 2010, 3S in August–September–October 2010, Table 2, and 4A in August 2012, Table 1). All the events were intense (mean SSS ∼ 33) and each lasted from 5 to 16 weeks (see Tables 1 and 2). Each of these winter events was preceded by the most intense wind reversals observed between 2010 and 2014 (Figures 7c and 7d). We argue that these wind reversals from southwesterly to northeasterly winds caused the offshore expansion of RdlP waters, thus providing a more intense export of low-salinity waters along the coast of southern Brazil, and a stronger salinity anomaly in the open ocean. The export of shelf waters to the open ocean creates extensive negative salinity anomalies (<-0.5) over the southward flowing Brazil Current between 27°S and 35°S (Figures 10a and 10b). Likewise, in winter the numerical simulations present extensive negative salinity anomalies in the open ocean north of about 36°S [*Matano et al*., 2014, Figure 10]. Given the relatively high sea surface temperatures advected within the Brazil Current, similar features are probably the source of the warm variety of low-salinity waters reported in previous studies [*Gordon*, 1989; *Piola et al*., 2008b].

Earlier observations of low-salinity waters around the BMC and on the continental shelf off Uruguay and southern Brazil have been associated with large RdlP outflow events [e.g., *Provost et al*., 1996; *Campos et al*., 1999]. In contrast, historical data and numerical simulations [*Piola et al*., 2005] and evidence from the analysis a SSS proxy [*Piola et al*., 2008a] suggest that variations in the river discharge primarily influence the region offshore of the river mouth, while salinity variations over the shelf northeast of the estuary are mostly associated with alongshore wind stress variability. These results are in excellent agreement with the analysis of the modes of SSS variability in a numerical model [*Matano et al*., 2014]. In the model, the first mode of SSS variability is centered over the shelf, where seasonal SSS anomalies are well correlated with alongshore wind variations, while the second mode has maximum loadings east of the river mouth and is correlated with the river discharge.

5. Summary and Conclusions

We have carried out an extensive analysis of satellite-derived sea surface salinity in the southwest South Atlantic Ocean, with the aim of investigating the signals associated with the export of low-salinity shelf waters to the open ocean. Despite the low spatial resolution compared to other satellite sensors and land contamination issues which prevent their use near land, our results suggest that Aquarius and SMOS capture the detrainment of shelf waters, and, for the first time, provide observations to test hypotheses about their fate in the open ocean and to validate numerical simulations. The export of shelf waters near the RdlP causes the strongest salinity signal throughout the South Atlantic, excluding the tropics. The detrainment of low-salinity waters present a strong seasonal signal which is associated with the alongshore wind stress variability over the shelf. The analysis shows that in austral summer mixtures of low-salinity shelf waters from the Rio de la Plata expand to the outer shelf and are detrained from the shelf near 36°S–37°S. The satellite

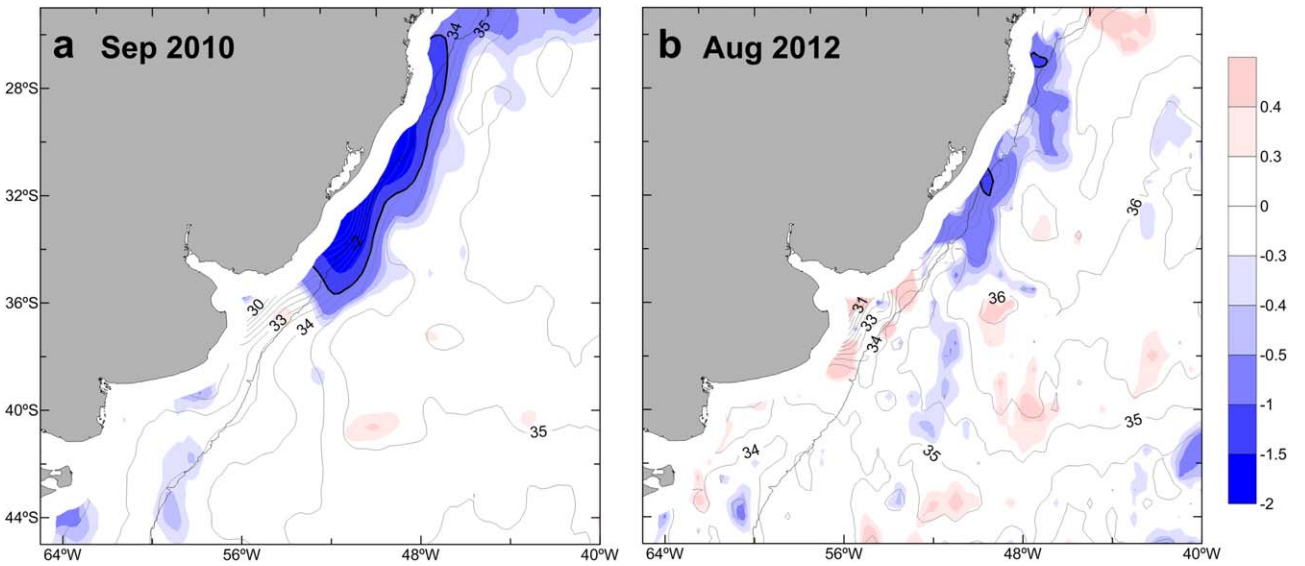

Figure 10. SSS (contours) and SSS anomaly (colors) for (a) September 2010 constructed from SMOS L2 data and (b) August 2012 constructed with Aquarius data, relative to the 2012–2013 mean. The gray thick line indicates the 200 m isobath.

data suggest that in the open ocean the low-salinity waters cause an extensive negative salinity anomaly whose core follows the path of the BMC. In winter the low-salinity waters are advected northeastward, forming a narrow coastal current and are exported to the open ocean farther north. As the winter export is distributed along the seaward edge of the low-salinity plume and mix with salty tropical waters carried by the Brazil Current the low-salinity signal is rapidly lost. Nevertheless, anomalous wind reversals toward the northeast in winter, act to expand the low-salinity waters offshore causing extensive low-salinity anomalies over the Brazil Current. The export of low-salinity shelf waters is likely to have a substantial impact on the vertical stratification and biochemical properties of the upper layer on this region. The satellite borne salinity observations are still not capable of detecting the export of subantarctic shelf water along the edge of the Patagonia shelf, as its salinity is too close to the neighboring Malvinas Current. Given the relatively coarse resolution of the present-day generation of satellite salinity radiometers that observe portions of the ocean surface at scales of several tens of kilometers, it is possible that the actual export patterns are significantly narrower and lower in salinity than depicted by the satellites, as suggested by satellite color images and high-resolution numerical simulations. However, the general agreement with the numerical simulations and in situ observations indicate an outstanding overall performance of the satellite-based salinity sensors.

References

Bonjean, F., and G. S. E. Lagerloef (2002), Diagnostic model and analysis of the surface currents in the tropical Pacific Ocean, *J. Phys. Oceanogr.*, *32*, 2938–2954.

Borús, J., M. Uriburu Quirno, and D. Calvo (2013), *Evaluación de caudales diarios descargados por los grandes ríos del sistema del Plata al estuario del Río de La Plata*, Alerta hidrológico-Inst. Nac. del Agua y el Ambiente, Ezeiza, Argentina.

Campos, E. J. D., C. A. D. Lentini, J. L. Miller, and A. R. Piola (1999), Interannual variability of the sea surface temperature in the South Brazil Bight, *Geophys. Res. Lett.*, *26*, 2061–2064.

Campos, E. J. D., A. R. Piola, R. P. Matano, and J. L. Miller (2008), PLATA: A synoptic characterization of the southwest Atlantic shelf under influence of the Plata River and Patos Lagoon outflows, *Cont. Shelf Res.*, *28*, 1551–1555.

Campos, P., O. O. Möller, A. R. Piola, and E. D. Palma (2013), Seasonal variability and western boundary upwelling: Cape Santa Marta (Brazil), *J. Geophys. Res. Oceans*, *118*, 1420–1433, doi:10.1002/jgrc.20131.

Castro, B. M., and L. B. Miranda (1998), Physical oceanography of the western Atlantic continental shelf located between 4°N and 34°S, in *The Sea*, vol. II, edited by A. R. Robinson and K. H. Brink, chap. 8, pp. 209–251, John Wiley, N. Y.

Ciotti, A. M., C. Odebrecht, G. Fillman, and O. O. Möller Jr. (1995), Freshwater outflow and subtropical convergence influence on phytoplankton biomass on the Southern Brazilian Continental Shelf, *Cont. Shelf Res.*, *15*, 1737–1756.

Combes, V., and R. P. Matano (2014), A two-way nested simulation of the oceanic circulation in the Southwestern Atlantic, *J. Geophys. Res. Oceans*, *119*, 731–756, doi:10.1002/2013JC009498.

Emilson, I. (1961), The shelf and coastal waters off southern Brazil, *Bol. Inst. Oceanogr.*, *11*(2), 101–112.

Framiñan, M. B., M. P. Etala, E. M. Acha, R. A. Guerrero, C. A. Lasta, and O. B. Brown (1999), Physical characteristics and processes of the Río de la Plata Estuary, in *Estuaries of South America: Their Morphology and Dynamics*, edited by G. M. E. Perillo, M. C. Piccolo, and M. P. Quivira, pp. 161–194, Springer, Berlin.

Acknowledgments

We dedicate this article to the memory of Hermes W. Mianzan, whose insight and interest in the impact of cross-shelf exchanges on the ecology of the continental shelf was a major motivation for our study, he will be greatly missed. The hydrographic data are available at http://www.ceado.gov.ar, http://www.inidep.edu.ar, and http://www.nodc.noaa.gov/OC5/WOD13. Aquarius data are available at ftp://podaac.jpl.nasa.gov and SMOS data at http://cp34-bec.cmima.csic.es. OSCAR data are available at http://www.oscar.noaa.gov, ASCAT data at http://nesdis.noaa.gov, ocean color data at http://oceancolor.gsfc.nasa.gov/cgi/l3, and altimeter data at http://www.aviso.oceanobs.com. This research was funded by Comisión Nacional de Actividades Espaciales and Ministerio de Ciencia, Tecnología e Innovación Productiva, Argentina grant 001 to A.R.P., E.D.P., and M.S. and grant 008 to R.A.G. and H.F. In addition, A.R.P., M.S., and E.D.P. acknowledge the support of grants SGP2076 and CRN3070 from the Inter-American Institute for Global Change Research, through the US National Science Foundation grants GEO-0452325 and GEO-1128040 and the partial support of Agencia Nacional de Promoción Científica y Tecnológica (Argentina) through Grant PICT-2012-0467. M.S. also aknowledge the support of UMETSAT/CNES DSP/OT/12-2118 and CONICET-YPF PIO 133-20130100242. R.P.M. acknowledges the financial support of NASA through grants NNX08AR40G and NNX12AF67G, NOAA through grant NA13OAR4310132 and the National Science Foundation through grant OCE-0928348. P.T. Strub acknowledges the financial support of NASA through grants NNX08AR40G. Y.C. is funded by the NASA Ocean Salinity Science Team grant at UCLA through a subcontract to grant NNX08AR40G. We acknowledge the constructive criticism of two anonymous reviewers. This is INIDEP contribution N° 1900.

Gordon, A. L. (1989), Brazil–Malvinas Confluence—1984, *Deep Sea Res., Part A*, *36*, 359–384.

Guerrero, R. A., E. M. Acha, M. B. Framiñan, and C. A. Lasta (1997), Physical oceanography of the Río de la Plata Estuary, Argentina, *Cont. Shelf Res.*, *17*, 727–742.

Guerrero, R. A., A. R. Piola, G. N. Molinari, A. P. Osiroff, and S. I. Jauregui (2010), *Climatología de temperatura y salinidad en el Río de la Plata y su frente marítimo, Argentina-Uruguay*, 95 pp., Inst. Nac. de Invest. y Desarrollo Pesquero, Mar del Plata, Argentina.

Hamming, R. W. (1977), *Digital Filters*, Prentice-Hall, Upper Saddle River, N. J.

Jaime, P. R., and A. Menendez (2002), *Análisis del régimen hidrológico de los ríos Paraná y Uruguay, Informe Técnico Freplata*, INA LHA 05–216-02, 140 pp., Inst. Nac. del Agua, Ezeiza, Argentina.

Lilly, J. M., and G. S. E. Lagerloef (2008), Aquarius Level 3 processing algorithm theoretical basis document. Version 0.9., Aquarius Ground Segment, Goddard Space Flight Cent, Greenbelt, Md.

Matano, R. P., E. D. Palma, and A. R. Piola (2010), The influence of the Brazil and Malvinas Currents on the southwestern Atlantic shelf circulation, *Ocean Sci.*, *6*, 983–995, doi:10.5194/os-6-983-2010.

Matano, R. P., V. Combes, A. R. Piola, R. Guerrero, E. D. Palma, P. T. Strub, C. James, H. Fenco, Y. Chao, M. Saraceno (2014), The salinity signature of the cross-shelf exchanges in the southwestern Atlantic Ocean: numerical simulations, *J. Geophys. Res. Oceans*, *119*, doi: 10.1002/2014JC010116.

Meissner, T. (2014), Performance degradation and Q/C flagging of Aquarius L2 salinity retrievals, *RSS Tech. Rep. 031814*, Remote Sensing Systems, Santa Rosa, Calif.

Möller, O. O., Jr., A. R. Piola, A. C. Freitas, and E. J. D. Campos (2008), The effects of river discharge and seasonal winds on the shelf off Southeastern South America, *Cont. Shelf Res.*, *28*, 1607–1624.

Palma, E. D., R. P. Matano, and A. R. Piola (2004), A numerical study of the Southwestern Atlantic Shelf circulation: Barotropic response to tidal and wind forcing, *J. Geophys. Res.*, *109*, C08014, doi:10.1029/2004JC002315.

Palma, E. D., R. P. Matano, and A. R. Piola (2008), A numerical study of the Southwestern Atlantic Shelf circulation: Stratified ocean response to local and offshore forcing, *J. Geophys. Res.*, *113*, C11010, doi:10.1029/2007JC004720.

Pimenta, F. M., E. J. D. Campos, J. Miller, and A. R. Piola (2005), Numerical study of the Plata River plume along the southeastern South American continental shelf, *Braz. J. Oceanogr.*, *53*(3–4), 129–146.

Piola, A. R., E. J. D. Campos, O. O. Möller, M. Charo, and C. Martinez (2000), Subtropical shelf front off eastern South America, *J. Geophys. Res.*, *105*(C3), 6566–6578.

Piola, A. R., R. P. Matano, E. D. Palma, O. O. Möller, and E. J. D. Campos (2005), The influence of the Plata River discharge on the western South Atlantic shelf, *Geophys. Res. Lett.*, *32*, L01603, doi:10.1029/2004GL021638.

Piola, A. R., S. I. Romero, and U. Zajaczkowski (2008a), Space-time variability of the Plata plume inferred from ocean color, *Cont. Shelf Res.*, *28*, 1556–1567, doi:10.1016/j.csr.2007.02.013.

Piola, A. R., O. O. Möller Jr., R. A. Guerrero, and E. J. D. Campos (2008b), Variability of the subtropical shelf front off eastern South America: Winter 2003 and summer 2004, *Cont. Shelf Res.*, *28*, 1639–1648, doi:10.1016/j.csr.2008.03.013.

Provost, C., V. Garçon, and L. M. Falcon (1996), Hydrographic conditions in the surface layers over the slope-open ocean transition area near the Brazil–Malvinas confluence during austral summer 1990, *Cont. Shelf Res.*, *16*(2), 215–219.

Rio, M. H., S. Guinehut, and G. Larnicol (2011), New CNES-CLS09 global mean dynamic topography computed from the combination of GRACE data, altimetry, and in situ measurements, *J. Geophys. Res.*, *116*, C07018, doi:10.1029/2010JC006505.

Romero, S. I., A. R. Piola, M. Charo, and C. A. E. Garcia (2006), Chlorophyll-a variability off Patagonia based on SeaWiFS data, *J. Geophys. Res.*, *111*, C05021, doi:10.1029/2005JC003244.

Saraceno, M., C. Provost, and A. R. Piola (2005), On the relationship of satellite retrieved surface temperature fronts and chlorophyll-a in the Western South Atlantic, *J. Geophys. Res.*, *110*, C11016, doi:10.1029/2004JC002736.

Simionato, C. G., M. N. Nuñez, and M. Engel (2001), The salinity front of the Río de la Plata—A numerical case study for winter and summer conditions, *Geophys. Res. Lett.*, *28*(13), 2641–2644.

Simionato, C. G., W. Dragani, V. Meccia, and M. Nuñez (2004), A numerical study of the barotropic circulation of the Río de La Plata Estuary: Sensitivity to bathymetry, earth rotation and low frequency wind variability, *Estuarine Coastal Shelf Sci.*, *61*, 261–273.

Stevenson, M. R., D. Dias-Brito, J. L. Stech, and M. Kampel (1998), How do cold water biota arrive in a tropical bay near Rio de Janeiro, Brazil?, *Cont. Shelf Res.*, *18*(13), 1595–1612.

Vaz, A. C., O. O. Möller Jr., and T. L. de Almeida (2006), Análise quantitativa da descarga dos rios afluentes da Lagoa dos Patos, *Atlântica*, *28*(1), 13–23.